CLM-P583

CLM-P583

UKAEA

Preprint

HOLOGRAPHIC INTERFEROMETRY MEASUREMENT OF CONVECTIVE HEAT TRANSPORT BENEATH A HEATED HORIZONTAL PLATE IN AIR

R. E. FAW
T. A. DULLFORCE

CULHAM LABORATORY
Abingdon Oxfordshire

1979

HOLOGRAPHIC INTERFEROMETRY MEASUREMENT OF CONVECTIVE HEAT TRANSPORT BENEATH A HEATED HORIZONTAL PLATE IN AIR

by

R. E. Faw* and T. A. Dullforce

Culham Laboratory, UKAEA Research Group
Abingdon, Oxfordshire, England

Abstract

The technique of live-fringe holographic interferometry has been used in an investigation of convective heat transfer beneath a heated horizontal plate in air. Two copper plates were used, one a 5.1 cm square, the other a 16 cm square. Temperature profiles were measured in air beneath isothermal plate surfaces at Rayleigh numbers ranging from 4×10^4 to 1.5×10^6. The paper describes apparatus and procedures used in the holographic process as well as methods used in deriving temperature profiles from interferograms. Measured temperature profiles were in excellent agreement with predictions based on approximate analytical solutions to the heat transfer problem previously reported by others. Plate-average Nusselt numbers, derived from the measured temperature profiles, exceeded predicted values but were in accord with previous measurements.

*Present address: Nuclear Engineering Department, Kansas State University, Manhattan, Kansas, U.S.A.

Submitted for publication in Journal of Heat and Mass Transfer)
une, 1979.

Nomenclature

a	plate characteristic dimension (m)
b	plate dimension (m)
g	acceleration of gravity (m/s^2)
K	Gladstone-Dale constant (m^3/kg)
n	refractive index
Nu	Nusselt number
p	pressure (Pa)
R	ideal gas constant (m^3Pa/kgK)
Ra	Rayleigh number
T	temperature (K)
v	$z/\delta(0,y)$
X,Y,Z	spatial coordinates
x,y,z	X/a, Y/a, Z/a
α	thermal diffusivity (m^2/s)
β	coefficient of thermal expansion (K^{-1})
δ	dimensionless boundary layer thickness (2/Nu)
ε	fringe displacement
θ	$T - T_\infty$ (K)
λ	wavelength (m)
ν	kinematic viscosity (m^2/s)
ξ	$(1-x^2)\ (1-y^2)$
ρ	density (kg/m^3)
ϕ	$(T - T_\infty)/(T_o - T_\infty)$

Subscripts

o	conditions at heat transfer plate (z=0)
∞	ambient conditions

1. Introduction

Measurements have been made of convective heat transport in air beneath the surface of a horizontal square plate held at a constant temperature above that of the surroundings. Two plates were used, both made of copper, one a 5.1 cm square, the other a 16 cm square. Plate temperatures varied from 10 K to 50 K above the ambient temperature. Live-fringe holographic interferometry was used to measure temperature profiles from which were determined convective heat transfer coefficients and boundary layer thicknesses. Results were correlated in terms of the Nusselt number *vs* the Rayleigh number.

Figure 1 establishes the geometrical notation used here. Within the fluid, the dimensionless temperature index is

$$\phi(x,y,z) = \theta(x,y,z)/\theta_o \tag{1}$$

in which θ_o is the plate temperature T_o less the ambient temperature T_∞, and $\theta(x,y,z)$ is the local fluid temperature $T(x,y,z)$ less the ambient temperature. Dimensionless position indices are defined in terms of the characteristic plate dimension, *viz* $x = X/a$. The Rayleigh and Nusselt numbers, defined in terms of the same characteristic length, are respectively

$$Ra = g\beta a^3 \theta_o/\alpha\nu, \tag{2}$$

$$Nu(x,y) = -\frac{\partial\phi}{\partial z}(x,y,0) \quad . \tag{3}$$

Average Nusselt numbers of interest are

$$\overline{Nu}(y) = \int_0^1 dx\ Nu(x,y) \quad , \tag{4}$$

and

$$\overline{\overline{Nu}} = \int_0^1 dy \int_0^1 dx\ Nu(x,y) \quad . \tag{5}$$

A dimensionless index of the boundary layer thickness may be defined as

$$\delta(x,y) = 2/Nu(x,y) \quad . \tag{6}$$

Similarly,

$$\overline{\delta}(y) = 2/\overline{Nu}(y) \quad . \tag{7}$$

Experimental studies of downward heat transfer by convection from horizontal surfaces have built upon the early efforts of Weise[1], Saunders, Fishenden and Mansion[2], and Kraus[3], whose investigations had established that, over a wide range of parameters, the Nusselt number for heat transfer was proportional to the 0.2 power of the Rayleigh number, and only weakly dependent on the surface shape and edge conditions. Recent experimental studies include the work of Fujii and Imura[4] and Aihara, Yamada and Endo[5]. The former measured average Nusselt numbers for heat transfer to water from rectangular brass plates 5 cm x 10 cm x 0.5 cm thick and 15 cm x 30 cm x 1 cm thick. In an effort to establish two-dimensional flow patterns, the plate sides were insulated along the shorter dimensions (Y = ± b in Fig. 1). The uninsulated sides were presumably at or near the plate surface temperature. Over the range $10^6 \leq Ra \leq 10^{11}$ boundary layer flow was found to be laminar, with

$$\overline{Nu}(y) = 0.58\ Ra^{0.2} \quad . \tag{8}$$

Note that this is an average over the X coordinate, with the b dimension assumed to be infinite.

Aihara and his co-workers studied heat transfer to air from a brass plate 25 cm x 35 cm x 1 cm thick. The shorter sides of the plate were insulated and the uninsulated sides were presumably at or near the plate surface temperature. With reference to Fig. 1, a thermocouple probe was used to measure $\phi(0,y,z)$ for $0 \leq y \leq 1$. Except for $y > 0.8$, observed temperature profiles were represented well by the equation

$$\phi(0,y,z) = [1+z/\delta(0,y)][1-z/\delta(0,y)]^3 \ . \qquad (9)$$

Temperature profiles and local Nusselt numbers were in substantial agreement with those predicted by Singh and Birkebak[6] for an infinite strip (see below).

Birkebak and Abdulkadir[7] investigated heat transfer to water from a square aluminium plate 19 cm on a side and 1.25 cm thick. By a special cooling system, plate sides were held at ambient temperature. Using a thermocouple probe, values of $\phi(0,y,z)$ were measured for y = 0, 0.5 and 0.85. Except near the edges of the plate, temperature profiles and local Nusselt numbers were in agreement with predictions of Singh, Birkebak and Drake[8] for a square plate (see below). In agreement with previous observations,[1,2,3,5] the boundary-layer thicknesses were found to be finite at the plate edges. The average Nusselt number over the entire plate surface was found to be

$$\overline{\overline{Nu}} = 0.68\ Ra^{0.2} \ . \qquad (10)$$

Restrepo and Glicksman[9] studied heat transfer to air from a copper plate 7 in x 7 in x 1 in thick with side surfaces (1) insulated, (2) heated to the plate surface temperature, or (3) cooled to ambient temperature. Temperature profiles $\phi(0,y,z)$ were measured using a thermocouple probe. At the plate edges, boundary layer thicknesses were much greater for the cooled sides than for the heated sides and for the former were as thick as 1/8 the plate dimensions. For plates with heated sides, plate-average Nusselt numbers agreed with Eq. (8).

Analytical studies of downward convection from plates have been carried out using the boundary-layer approximation. Stewartson[10] and Gill, Zeh and del Casal[11] obtained similarity solutions for a two-dimensional case. Integral methods were applied by Levy[12] and Wagner[13] for the semi-

infinite strip. The method was extended by Singh, Birkebak, and Drake[8] to rectangular and circular plates. These analyses involved assuming the thermal boundary layer to vanish at the plate edge. For the special case of the infinite strip, Singh and Birkebak[6] were able to obtain solutions accommodating finite boundary-layer thicknesses at the plate edge.

For the rectangular plate, the subject of this experimental study, the analysis of Singh, Birkebak and Drake[8] leads to temperature profiles of the form

$$\phi(x,y,z) = [1 - \frac{z}{\delta(x,y)}]^2 \tag{11}$$

in which, to a first-order approximation,

$$\delta(x,y,) = \delta_o \xi^{1/4}(x,y) \tag{12}$$

with

$$\delta_o = \delta(0,0) = 4.357\ Ra^{-1/5} \tag{13}$$

and

$$\xi(x,y) = (1-x^2)(1-y^2)\ . \tag{14}$$

The local Nusselt number is thus

$$Nu(x,y) = 2/\delta(x,y) = 0.459\ \xi^{-1/4}(x,y)\ Ra^{1/5} \tag{15}$$

2. Experimental Procedure

Measurements were made of temperature profiles in air beneath the surface of a heated, downward-facing, horizontal plate using live-fringe holographic interferometry. A general discussion of the technique and apparatus has been described elsewhere[14]. Using an argon-ion laser, a hologram was made of the plate and its surroundings, all at ambient temperature. The plate temperature was then increased, while the hologram and plate were illuminated by the laser light under conditions

otherwise identical to those during the preparation of the hologram. The holographic image was superimposed on the real plate and surroundings. Changes in refractive index of the heated air led to optical interference patterns which were recorded photographically. From the interference patterns were determined temperature profiles. With reference to Fig. 1, the temperatures measured were averages over the x coordinate, i.e.,

$$\bar{\phi}(y,z) = \int_0^1 dx\ \phi(x,y,z) \ . \tag{16}$$

From the temperature profiles were derived the average Nusselt numbers $\overline{Nu}(y)$ and $\overline{\overline{Nu}}$.

The overall arrangement of apparatus is illustrated in Fig. 2. Apparatus was positioned on a granite bench, 4 ft x 10 ft x 4 in thick. Isolation from vibration was provided by supporting the bench at each corner on lightly inflated rubber-tyre inner tubes. The tubes rested on sand-filled concrete cylinders. The cylinders rested on a sand base in larger concentric concrete cylinders, also sand-filled. (For further details, see ref. 14).

The beam from an argon-ion laser was elevated to 26 cm above the bench by a pair of beam positioning mirrors. After passing through a shutter, the beam was divided into two equal components by a beam-splitting cube. One beam, the reference beam, was expanded by a 20X microscope objective and filtered by an 11μm diameter pin-hole. The objective was located 85 cm from the hologram plate and the expanded beam struck the plate at an angle of about 45°. A second beam, the object beam, was expanded and filtered by a 20X objective and 11μm pin-hole and collimated by a 15 cm diameter, 50 cm focal length lens located 38 cm from the center of the heat transfer plate. A variable

density filter was used to adjust the intensity of the object beam. The X-axis of the heat transfer plate (Fig. 1) was aligned with the axis of the object beam.

The laser used was a high-power, argon-ion laser, Spectra-Physics Model 171-06. It had a nominal power rating of 9W (multi-line) and 3.75W (514.5 nm-line). Available power was considerably in excess of rated power. Single-frequency operation was made possible by the use of an etalon, Spectra-Physics Model 589, in the laser cavity. With the etalon in use, available power at 514.5 nm was about 2.5 W. Laser beam diameter (e^{-2} points) was nominally 1.6 mm with a full-angle beam divergence of 0.72 mrad.

Mirrors, beam expanders, positioners, splitters, and spatial filters were components distributed by Ealing-Beck, Ltd. For high-power operation, uncemented microscope objectives, manufactured by W. R. Prior, were used. The reference-beam mirror was a 4 in diameter Schlieren-quality mirror made by Optical Works Ltd. The hologram plate holder was a Micro-Controle, Type SH37 Plate Support distributed by Unimatic Engineers Ltd. Hologram plates were 8E56 (AHI) Holotest Plates made on special order by Agfa-Gevaert Ltd. The plates were 4 in x 5 in with thickness 1.5-1.7 mm. Plate flatness is 10 μm/cm or better.

Two heat-transfer plates were used. One was a square copper plate, 16 cm on a side and 1.25 cm thick. Thermocouple wells, 1.25 mm diameter, were drilled to 1 mm from the plate surface. Sixteen wells were located within one quarter-sector of the plate. The plate was heated by four independent nichrome heating elements encased in ceramic insulating tubes recessed into grooves in an insulating backing plate (resin-impregnated fibre-board). The backing plate was square, 15.8 cm on a side, and was slightly smaller than the heat-transfer plate, so as not to disturb flow

around the edge of the heat-transfer plate. The heating elements were in an array of concentric squares spaced to provide approximately uniform heating. The elements were individually powered through variable transformers connected to 240 V, 50 Hz mains power. To facilitate adjustment, variable resistors (22 ohm, 10 amp rating) were placed in series with the heating elements. With these arrangements, the plate temperature was easily held uniform to within 0.5 K. The second plate was also square, 5.1 cm on a side and 1 cm thick, backed by a 5 cm square insulating plate. Nichrome heating elements, in an array of three concentric squares, were placed in ceramic insulating tubes and positioned in recessed grooves in the backing plate. The elements were connected in series. Plate temperature was monitored by three thermocouples placed in 1.25 mm diameter wells drilled in the copper plate to 0.5 mm from the downward-facing surface.

The test plate was levelled and aligned using the horizontal unexpanded object beam from the laser. The laser beam was also used to align the camera used to photograph interference patterns. With the alignment beam along the centre-line of the plate, the leveled camera was positioned so that the beam passed through the aperture at its smallest stop and through the centre of the film-holder. To minimize effects of air currents, the test plate was surrounded on four sides by a glass-windowed enclosure made of heavy cardboard. The enclosure was open at the top and had air entrance slits at its base.

With the heat transfer plate at ambient temperature, a hologram plate was exposed to an incident energy density of about 5 $\mu J/cm^2$, with the intensity of the reference beam twice that of the object beam. The hologram plate was processed using a procedure similar to that described by Phillips and Porter[15]. The essential features were

development in undiluted Neofin Blau (Tetenal Photowerk), and bleaching in an aqueous solution of ferric nitrate, potassium bromide, and isopropanol.

With the heat-transfer test plate still at ambient temperature, the hologram plate was carefully repositioned in its holder and illuminated by the object and reference beams. A virtual holographic image of the test plate then appeared superimposed on the actual plate. The hologram plate was then displaced slightly to produce a system of parallel interference fringes (see Fig. 4), the so-called finite-fringe setting. Power was then applied to the heating elements of the test plate. The plate temperature was increased at a rate of about 1 K per minute while carefully monitoring the plate temperature to assure uniformity. Convective heat transfer from the plate caused density changes and corresponding refractive index changes in the air. These changes caused optical interference leading to distortion of the fringes.

Interference patterns were photographed on microfilm (Eastman Kodak 5669 Micro-File) using a 35-mm single lens reflex camera (Asahi Pentax KX) with a 50-mm focal length f/1.7 lens, augmented by a 15-cm diameter, 60-cm focal length lens (Tropel 280-150). Typical exposure time was 1/250 s with the laser power at 50 mW. The microfilm was processed using Teknol developer (May & Baker Ltd.).

3. Data Analysis

Raw experimental data were in the form of photographic records of interference patterns. Figure 3 is an interferogram for the 16 cm square plate, with θ_o = 10 K. This corresponds to the infinite fringe setting of the Mach-Zehnder interferometer and was produced by double-exposure holographic interferometry. The dark interference fringes may

be interpreted as isotherms in the air surrounding the test plate. This infinite fringe setting was difficult to achieve experimentally, and an alternate approach was used, the finite fringe setting.

Figure 4 exhibits deliberately introduced finite fringes for the 16 cm plate with $T_o = T_\infty = 294$ K, i.e., $\theta_o = 0$ K. The hologram plate was exposed under the prescribed conditions, but rotated very slightly about its vertical axis when re-positioned in its holder. Figure 5 exhibits the interferogram after the plate temperature had been brought to 334 K ($\theta_o = 40$ K). Adjacent pairs of light or dark fringes result from a change of one wavelength (514.5 nm) in the optical path length of the object beam between the conditions when the hologram was made and the conditions under observation. Differences between the interferograms of Figs. 4 and 5 are due to density changes in the air beneath the plate. Superposition of Figs. 4 and 5, shown schematically in Fig. 6, allows measurement of fringe displacement $\varepsilon(y,z)$ as a function of position, as well as the displacement ε_o at the plate surface. Figure 7 shows the loci of fringe displacements for Figs. 4 and 5. The procedure for determining fringe displacement was as follows. Prints of the microfilm records were made on Eastman Kodak 4556 Reproduction Film at an enlargement of about three times actual size. Films for Figs. 4 and 5, for example, were superimposed over an illuminated background and values of $\varepsilon(y,z)$ were scaled directly from the films.

Temperature profiles were determined from fringe displacements in the following manner. Since unit fringe displacement results from a change of one wavelength in optical path, the measured displacement is related to the variation in refractive index $n(x,y,z)$ of the air by the equation

$$\varepsilon(y,z) = (2a/\lambda) \int_0^1 dx\ [n(x,y,z)-n_\infty] \tag{15}$$

in which n_∞ is the refractive index at ambient temperature. According to the Gladstone-Dale law, the variation with density ρ of the refractive index of a gas is closely approximated by the equation

$$\frac{dn}{dT} = K \frac{d\rho}{dT} \quad . \tag{16}$$

Assuming ideal gas behavior,

$$\frac{dn}{dT} = - \frac{Kp}{RT^2} \tag{17}$$

in which p is the ambient pressure, R the ideal gas constant, and K the Gladstone-Dale constant. Thus

$$n(x,y,z) - n_\infty = \frac{-Kp}{R} \left(\frac{1}{T_\infty} - \frac{1}{T(x,y,z)} \right) \tag{18}$$

and

$$\varepsilon(y,z) = \frac{-2aKp}{R\lambda} \int_0^1 dx \left(\frac{T(x,y,z)-T_\infty}{T_\infty T(x,y,z)} \right) \quad . \tag{19}$$

If in the denominator of the integral, the approximation is made that

$$T(x,y,z) \simeq \overline{T}\ (y,z) = \int_0^1 dx\ T(x,y,z) \ , \tag{20}$$

then

$$\varepsilon(y,z) = \frac{-2aKp}{R\lambda} \left(\frac{1}{T_\infty} - \frac{1}{\overline{T}(y,z)} \right) \tag{21}$$

and

$$\overline{\phi}(y,z) = \left(1 + \frac{T_o}{T_\infty} \left(\frac{\varepsilon_o}{\varepsilon(y,z)} - 1 \right) \right)^{-1} \quad . \tag{22}$$

For the experimental conditions of this work, the approximation of Eq. (20) leads to negligible error in $\overline{\phi}$ as z approaches zero, and at most one or two percent error in $\overline{\phi}$ near the outside of the boundary layer.

Although the x-averaged Nusselt number could be determined as

$$\overline{Nu}(y) = - \frac{\partial \overline{\phi}}{\partial z}(y,o) \tag{23}$$

it was more convenient to determine it as

$$\overline{Nu}(y) = 2 \frac{\partial}{\partial y} [1-\overline{\phi}^{1/2}]_{y=0} \tag{24}$$

from a graph of $1-\overline{\phi}^{1/2}$ *vs* z since that function is expected to be linear in z as z approaches zero, and to have zero intercept. The x-averaged, dimensionless boundary layer thickness is given by Eq. (7).

4. Experimental Results

For the larger test plate, three different experimental runs were made, each run beginning with the preparation of a hologram of the plate at ambient temperature. For each run, three photographs each were made and analyzed for the experimental conditions θ_o = 10, 20, 30, and 40 K. Thus, nine measurements of fringe displacements, or temperature profiles, were made for each experimental condition. Uncertainties were determined as estimates of the standard deviations of measured positions corresponding to a given fringe displacement or x-averaged air temperature. For the smaller test plate, only one experimental run was made, but three photographs each were made and analyzed for the experimental conditions θ_o = 30, 40 and 50 K.

Figure 8 illustrates typical data for air temperature, in dimensionless form, as a function of dimensionless distance beneath the test plate. Values of $\overline{Nu}(y)$ as a function of Rayleigh number are listed in Table I. Rayleigh numbers were evaluated at the mean of T_o and T_∞. Uncertainties in $\overline{Nu}(y)$ are based on conservative estimates of upper and lower limits in the slope of a plot of $1-\overline{\phi}^{1/2}$ *vs* z. Also listed in the table are plate average values, $\overline{\overline{Nu}}$. These were determined by trapezoidal

integration of $\overline{Nu}(y)$. Uncertainties are conservative estimates based on integrals over the extrema of uncertainties in $\overline{Nu}(y)$.

5. Discussion of Results

The analytical predictions of Singh, Birkebak, and Drake[8] provide a convenient context within which to discuss experimental results. From Eq. (9) the predicted temperature profile is

$$\overline{\phi}(y,z) = \int_0^1 dx\ \phi(x,y,z) = \int_0^{x_{max}(y)} dx\ [1-z/\delta(x,y)]^2 , \qquad (25)$$

in which $\delta(x,y)$ is given by Eq. (10), and x_{max} is the x location at which $z = \delta(x,y)$, i.e.,

$$x_{max} = \{1 - [z/\delta(0,y)]^4\}^{1/2} . \qquad (26)$$

In terms of the new variable $v = x/\delta(0,y)$,

$$\overline{\phi}(v) = \int_0^{(1-v^4)^{1/2}} dx\ [1-v/(1-x^2)^{1/4}]^2$$

$$= (1-v^4)^{1/2} + v^2\sin^{-1}(1-v^4)^{1/2}$$

$$-2^{3/2}v[2E(\cos^{-1}v, 2^{-1/2}) - F(\cos^{-1}v, 2^{-1/2})] , \qquad (27)$$

in which the elliptic integrals are defined as

$$E(\psi,k) = \int_0^{\psi} dx\ (1-k^2\sin^2 x)^{1/2} \qquad (28)$$

$$F(\psi,k) = \int_0^{\psi} dx\ (1-k^2\sin^2 x)^{-1/2} . \qquad (29)$$

In accord with Eq. (27), measured temperature profiles in the form $\overline{\phi}(v)$ were found to be independent of y. Average values are presented in Table II and illustrated in Fig. 9. In preparing the data, values

of $\delta(0,y)$ were determined from measured values of $\overline{\delta}(y)$ as described below. Uncertainties are estimates of the standard deviation of values measured at different y locations. As may be seen in the figure, measured temperatures agree well with the predictions of Eq. (27).

Nusselt numbers may be predicted from Eq. (27) as follows.

$$\overline{\overline{Nu}}(y) = -\frac{\partial\phi}{\partial z}(y,0) = -\frac{1}{\delta(0,y)}\frac{\partial\overline{\phi}}{\partial v}(0) \tag{30}$$

$$\frac{\partial\overline{\phi}}{\partial v}(0) = -2^{3/2}\left[2E(\pi/2,2^{-\frac{1}{2}}) - F(\pi/2,2^{-\frac{1}{2}})\right] = -2.396 \ . \tag{31}$$

Thus, making use of Eqs. (10-(12),

$$\overline{\overline{Nu}}(y) = \frac{2.396}{\delta(0,y)} = 0.550\ (1-y^2)^{-\frac{1}{4}}\ Ra^{1/5}. \tag{32}$$

From Eqs. (7) and (32),

$$\overline{\delta}(y) = 0.8347\ \delta(o,y) \ . \tag{33}$$

The predicted plate average Nusselt number is

$$\overline{\overline{Nu}} = \int_0^1 dy\ \overline{Nu}(y) = 0.659\ Ra^{1/5} \ . \tag{34}$$

Measured plate average Nusselt numbers, as a function of Rayleigh number are illustrated in Fig. 10 along with the prediction of Eq. (34). That measured values exceed predicted values is to be expected. The model on which the predictions are based does not account for the finite boundary layer thickness at the edge of the heat transfer plate.

Uncertainties in measured values are relatively large - 5 to 10 percent. These are in part statistical and in part due to the difficulty in measuring the derivative of the temperature profile near the plate surface. Certain systematic errors are included in the uncertainties, namely uncertainties of ± 0.3 K in θ_o. Other possible systematic errors are not accounted for. These would include refraction errors and errors introduced in fringe displacement by the finite boundary layer thickness

at the plate edge. However, in the procedure used in evaluating temperature profiles, Eq. (22), only ratios of fringe displacement are involved, and these errors would therefore be minimized.

6. Acknowledgements

The continued support of the UKAEA Safety and Reliability Directorate, Culcheth, is gratefully acknowledged. We would also like to thank N. Boucher and R. Davies for their help in constructing apparatus.

References

1. Weise, R., Wärmeübergang durch freie Konvektion an quadratischen Platten," Forsch. auf Gebiet Ing; 6, 281-292 (1935).

2. Saunders, O. A., Fishenden, M., and Mansion, H. D., "Some measurements of convection by an optical method," Engineering, 483-85 (May 1935).

3. Kraus, W., "Temperatur- und Geschwindigkeitsfeld bei freier Konvektion um eine waagerechte quadratische Platte, "Physik Zeits, 4, 126-150 (1940).

4. Fujii, T., and Imura, H., "Natural convection heat transfer from a plate with arbitrary inclination," Int. J. Heat Mass Transfer, 15, 755-767 (1972).

5. Aihara, T., Yamada, Y., and Endo, S., "Free convection along the downward-facing surface of a heated horizontal plate," Int. J. Heat Mass Transfer, 15, 2535-2549 (1972).

6. Singh, S. N., and Birkebak, R. C., "Laminar free convection from a horizontal infinite strip facing downwards," Z.A.M.P., 20, 454-461 (1969).

7. Birkebak, R. C., and Abdulkadir, A., "Heat transfer by natural convection from the lower side of finite horizontal heated surface," Fourth International Heat Transfer Conference, Paris, Vol. 4, Paper NC2.2, (1970).

8. Singh, S. N., Birkebak, R. C., and Drake, R. M. Jr., "Laminar free convection heat transfer from downward-facing horizontal surfaces of finite dimensions," Progr. in Heat and Mass Transfer, vol. II, Pergamon Press, 1969, pp. 87-98.

9. Restrepo, F., and Glicksman, L. R., "The effect of edge conditions on natural convection from a horizontal plate," Int. J. Heat Mass Transfer, 17, 135-142 (1974).

10. Stewartson, K., "On the free convection from a horizontal plate," Z.A.M.P, 9a, 276-282 (1958).

11. Gill, W. N., Zeh, D. W., and del Casal, E., "Free convection on a horizontal plate," Z.A.M.P., 16, 539-541 (1965).

12. Levy, S., "Integral methods in natural-convection flow," J. Appl. Mech., 22, 515-522 (1955).

13. Wagner, C., "Discussion on integral methods in natural convection flow," J. Appl. Mech., 23, 320-321 (1956).

14. Faw, R. E., and Dullforce, T. A., "Holographic interferometry principles and procedures," Report CLM-RR/S2/19, Culham Laboratory, UKAEA Research Group, Abingdon, Oxfordshire, March 1977.

15. Phillips, N. J., and D. Porter, "An advance in the processing of holograms," J. Phys. E., Sci. Inst., 9, 631-634 (1976).

Table I. Measured values of $\overline{Nu}(y)$ and $\overline{\overline{Nu}}$ as functions of the Rayleigh number.

				$\overline{Nu}(y)$ at y =						
a(cm)	θ_o(K)	Ra	$\overline{\overline{Nu}}$	0	0.5	0.6	0.8	0.9	0.95	1.0
2.55	30	3.94×10^4	6.5 ± 0.4	5.3 ± 0.2		5.9 ± 0.2	6.3 ± 0.5	7.5 ± 0.5		17.8 ± 3.2
	40	4.87×10^4	7.2 ± 0.8	5.6 ± 0.5		6.3 ± 0.6	7.4 ± 0.9	9.6 ± 1.2		17.7 ± 3.8
	50	5.64×10^4	7.4 ± 0.8	6.0 ± 0.5		6.7 ± 0.6	7.7 ± 0.6	9.4 ± 1.4		15.3 ± 3.8
8.0	10	4.88×10^5	9.1 ± 0.6	7.7 ± 0.4	8.1 ± 0.3		9.6 ± 0.3	11.3 ± 0.2	13.5 ± 0.5	20.1 ± 2.5
	20	8.96×10^5	11.9 ± 0.5	10.1 ± 0.3	11.2 ± 0.4		12.4 ± 0.5	14.0 ± 0.5	15.9 ± 1.1	21.9 ± 3.0
	30	1.24×10^6	12.3 ± 0.6	10.8 ± 0.6			12.2 ± 0.5	13.7 ± 0.5	16.0 ± 0.9	24.2 ± 3.0
	40	1.53×10^6	13.5 ± 0.7	12.3 ± 0.9			13.0 ± 0.5	15.5 ± 0.6	18.3 ± 0.7	25.2 ± 1.7

Table II. Composite values of $\phi(v)$ averaged over the test plate.

a(cm)	θ_o(K)	Ra	$\phi(v)$	v
2.55	30	$3.9x \times 10^4$	0.369	0.308 ± .008
			0.565	0.205 .003
			0.767	0.108 .003
	40	4.87×10^4	0.270	0.393 ± .011
			0.413	0.293 .006
			0.561	0.210 .004
			0.714	0.138 .003
			0.874	0.064 .009
	50	5.63×10^4	0.204	0.479 ± .009
			0.422	0.296 .005
			0.537	0.210 .013
			0.657	0.152 .002
			0.781	0.093 .002
8.00	10	4.88×10^5	0.330	0.356 ± .013
			0.497	0.247 .003
			0.667	0.147 .012
			0.838	0.085 .007
	20	8.96×10^5	0.163	0.518 ± .017
			0.330	0.348 .010
			0.501	0.227 .024
			0.675	0.147 .003
			0.854	0.078 .008
	30	1.24×10^6	0.110	0.603 ± .027
			0.222	0.438 .006
			0.336	0.335 .006
			0.453	0.261 .010
			0.575	0.199 .006
			0.696	0.144 .003
			0.822	0.085 .005
			0.950	0.026 .002
	40	1.53×10^6	0.082	0.691 ± .021
			0.166	0.525 .015
			0.252	0.429 .012
			0.340	0.355 .009
			0.430	0.293 .008
			0.522	0.235 .005
			0.617	0.182 .004
			0.713	0.131 .004
			0.812	0.085 .003
			0.914	0.039 .004

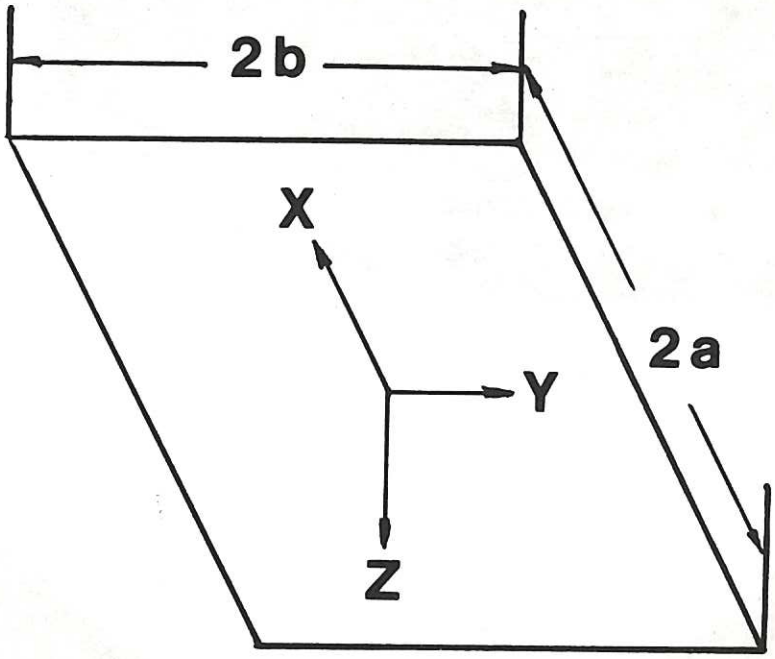

Fig.1 Geometry for the downward heat transfer experiment. The plate surface temperature is T_o. Ambient temperature is T_∞.

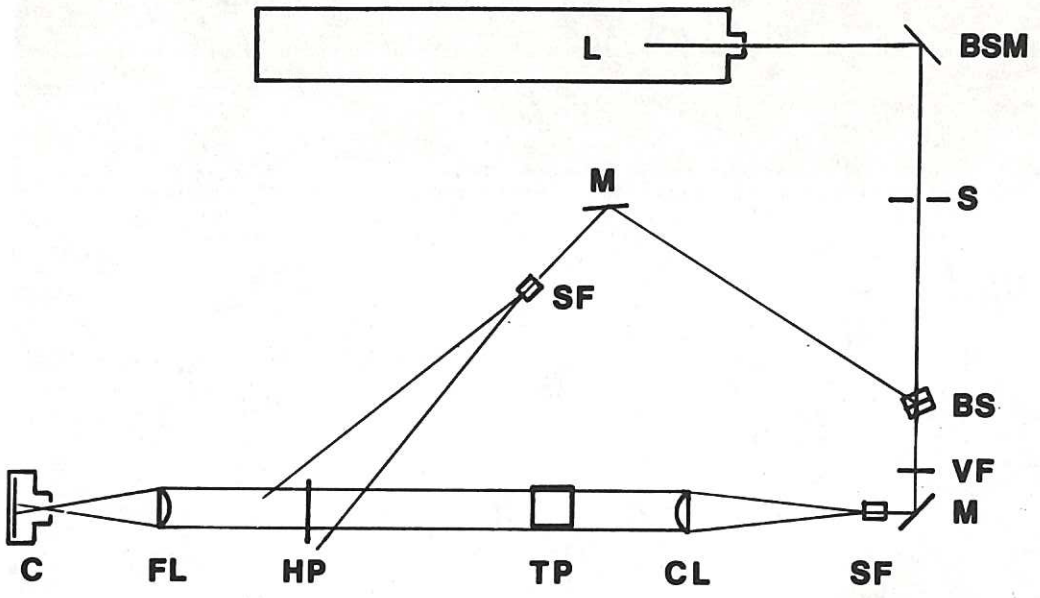

Fig.2 Experimental arrangement for holographic interferometry. L = laser, BP = beam positioning mirrors, S = shutter, BS = beam splitter, M = mirror, VF = variable filter, SF = spatial filter, CL = collimating lens, TP = heat transfer test plate, HP = hologram plate, FL = focusing lens, C = camera.

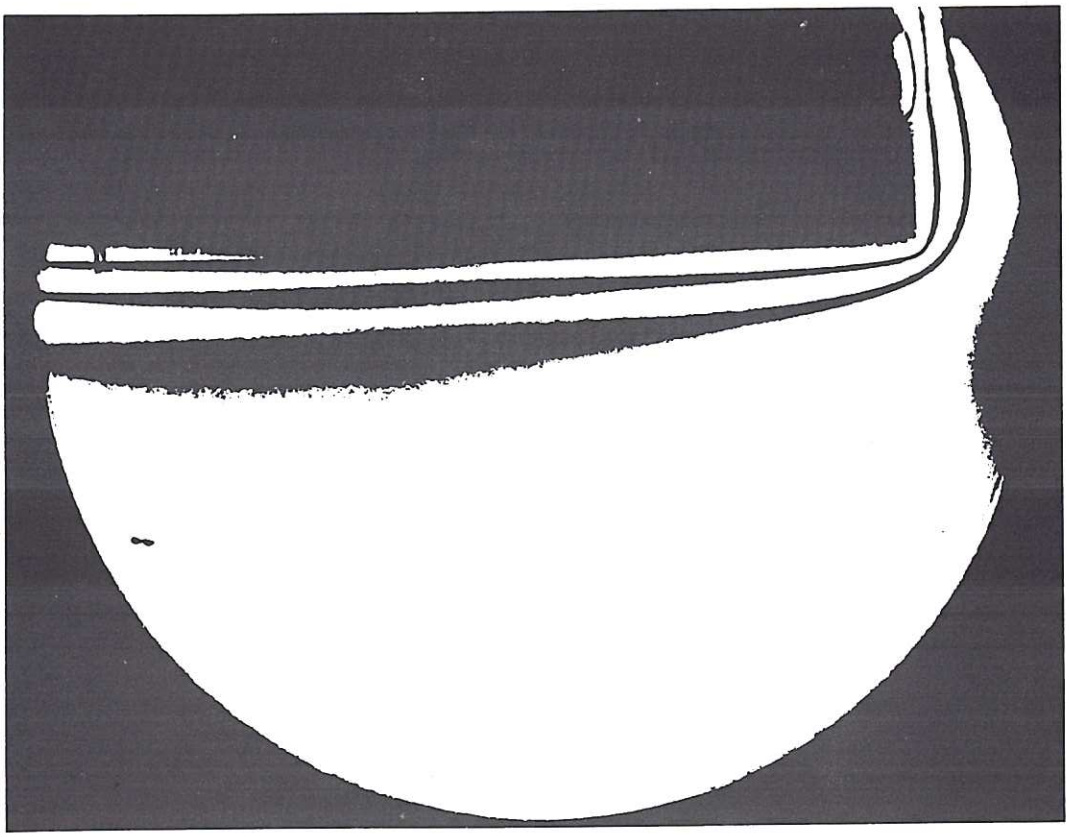

Fig.3 Infinite fringe interferogram for the 16cm plate with θ_o = 10K.

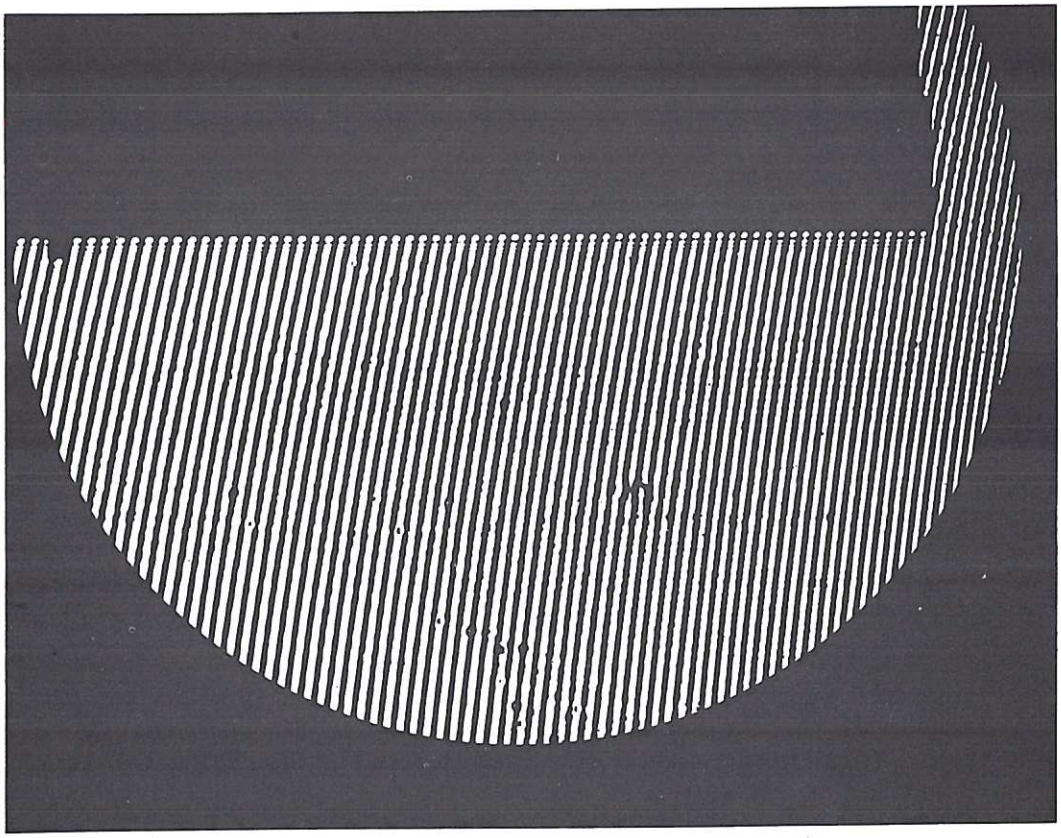

Fig.4 Finite fringe interferogram for the 16cm plate, with θ_o = 0K.

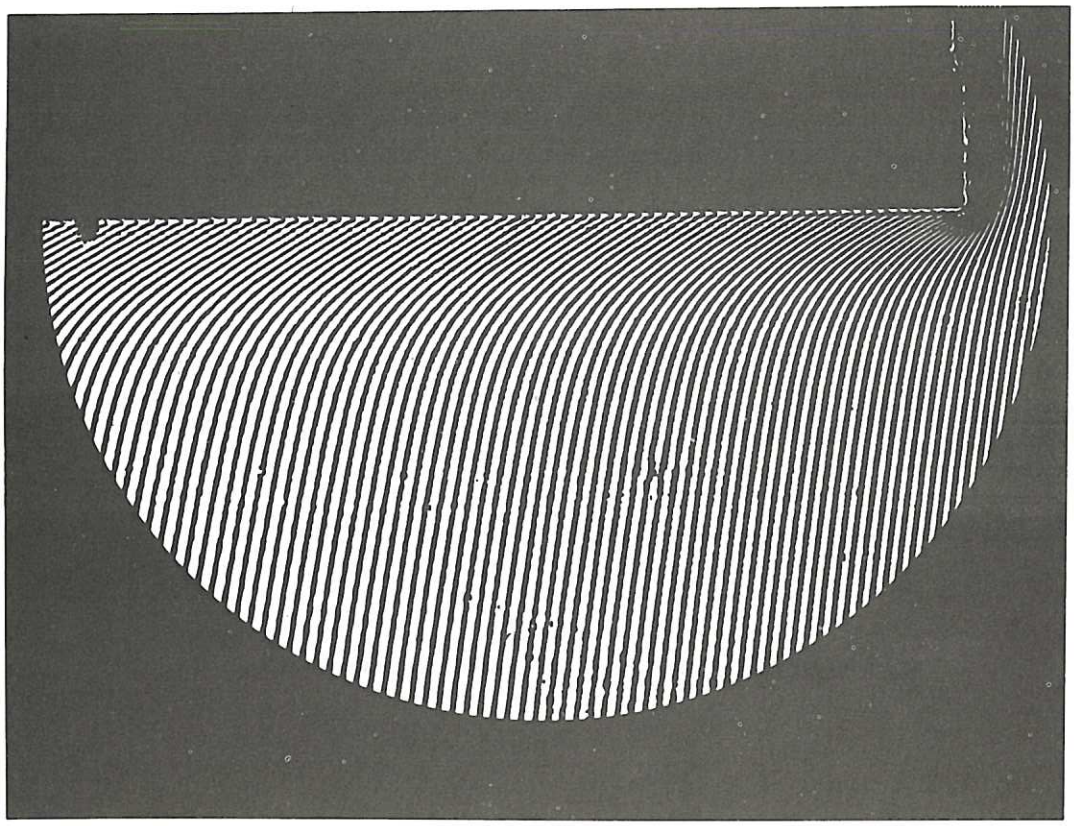

Fig.5 Finite fringe interferogram for the 16 cm plate, with θ_o = 40 K.

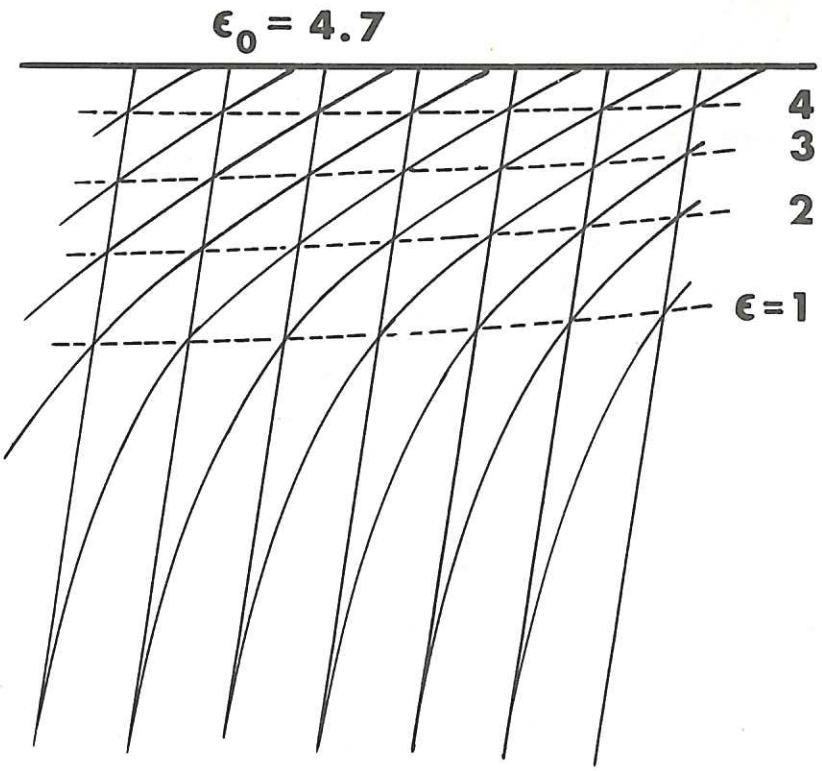

Fig.6 Superposition of interferograms to determine fringe displacement.

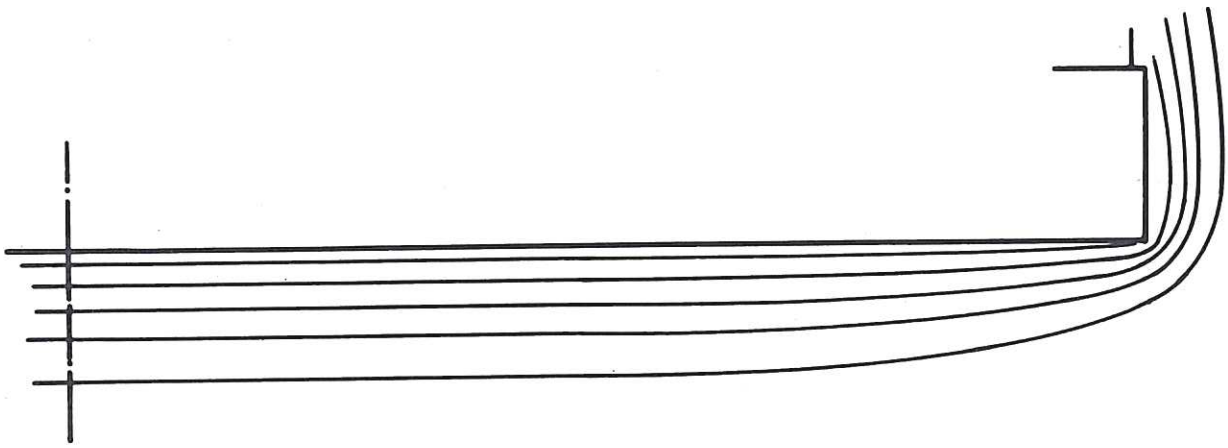

Fig.7 Loci of fringe displacements for the 16cm plate, with θ_0 = 20K.

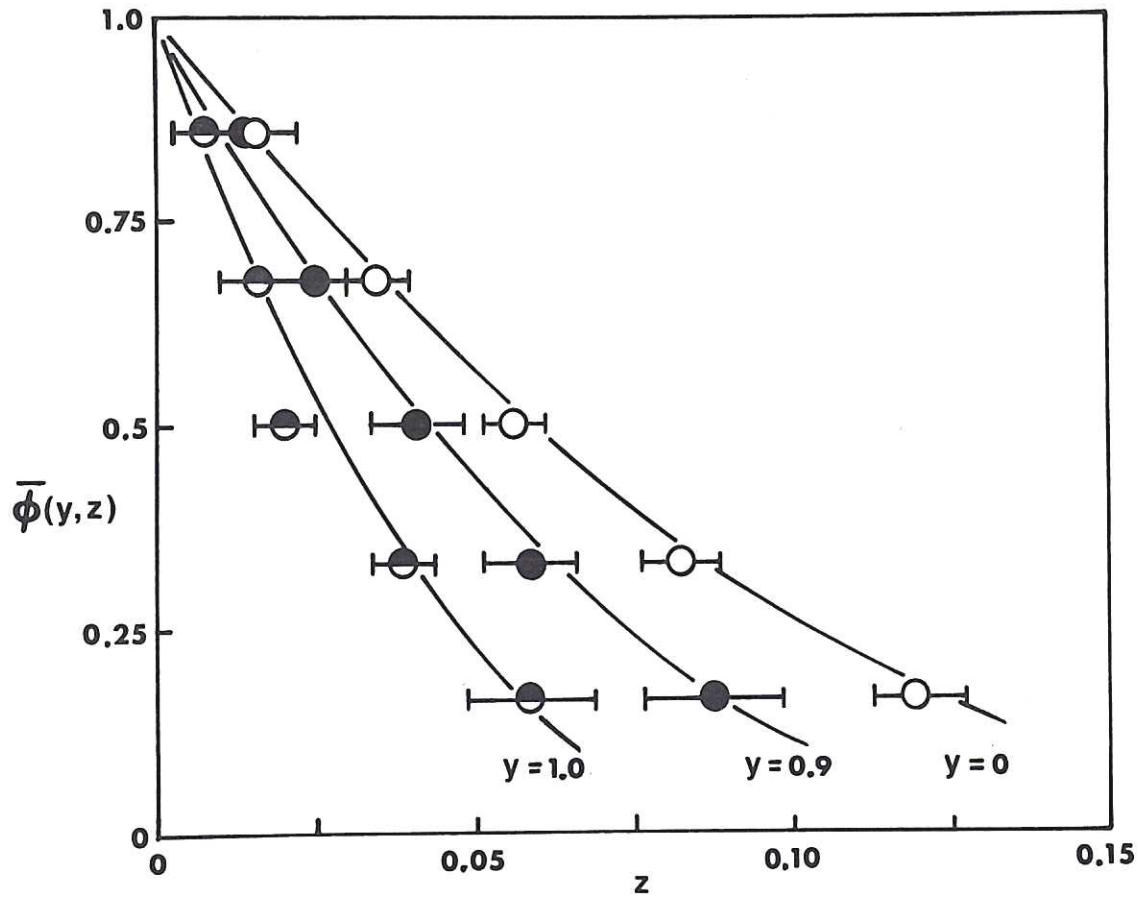

Fig.8 Air temperature $\overline{\phi}$ = (T-T$_\infty$)/(T$_0$-T$_\infty$) as a function of distance z = Z/a beneath the 16cm plate, with θ_0 = 20K. The solid lines are based on Eq.(27).

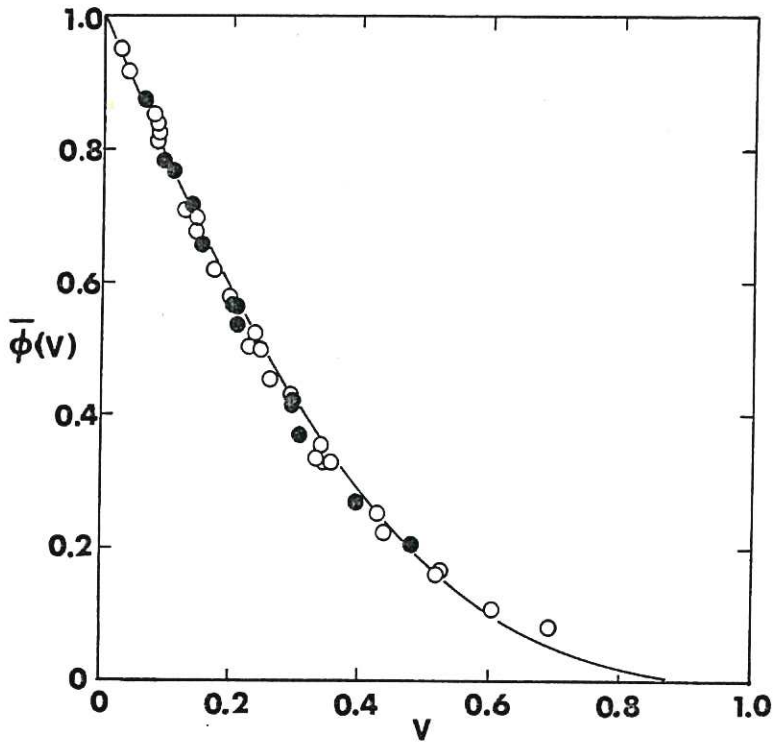

Fig.9 Composite data for $\overline{\phi}$(v). The solid line is Eq.(27). Open circles are for the 16cm test plate. Closed circles are for the 5·1 cm plate.

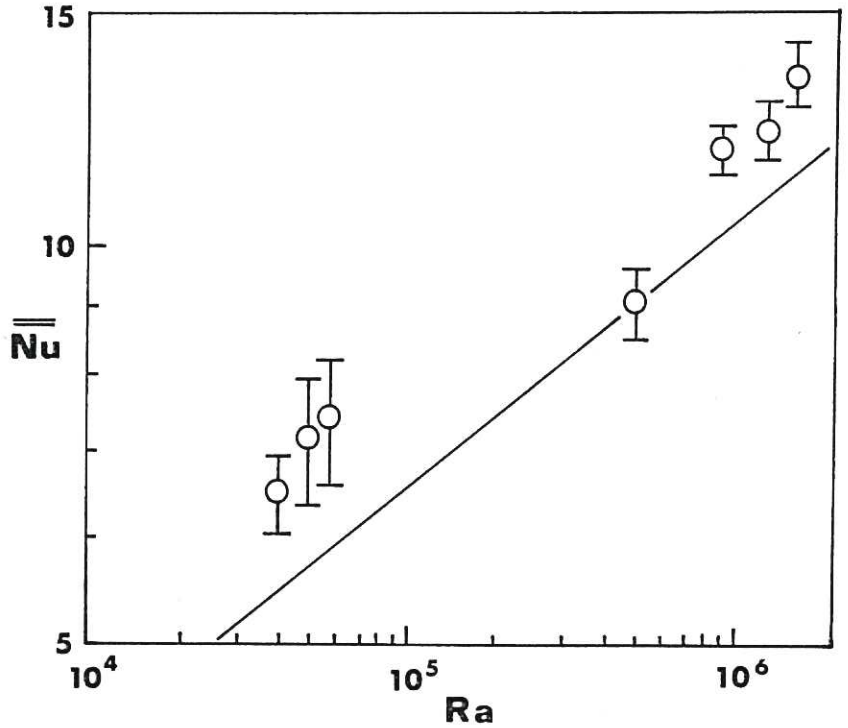

Fig.10 Plate average Nusselt number as a function of Rayleigh number. The solid line is Eq.(34).